Journal of Physics: Conference Series **527** (2014) 012009 doi:10.1088/1742-6596/527/1/012009

News on the equation of state from heavy ion reactions

M Colonna[1], V Baran[2], M Di Toro[1,3]

[1]Laboratori Nazionali del Sud, INFN, via Santa Sofia 62, I-95123, Catania, Italy
[2]Physics Faculty, University of Bucharest, Romania
[3]Physics-Astronomy Department, University of Catania, Italy

E-mail: colonna@lns.infn.it

Abstract. We discuss recent results on heavy ion reactions between charge asymmetric systems, from low up to intermediate energies. The theoretical framework is provided by mean-field based transport approaches. We focus on isospin sensitive observables, aiming at extracting information on the density dependence of the isovector part of the nuclear effective interaction and of the nuclear symmetry energy. For reactions close to the Coulomb barrier, we explore the structure of collective dipole oscillations, rather sensitive to the low-density behavior of the symmetry energy. At intermediate energies, where regions with higher density and momentum are reached, we discuss collective flows and their sensitivity to the momentum dependence of the isovector interaction channel, which determines the splitting of neutron and proton effective masses.

1. Introduction

The behavior of nuclear matter in several conditions of density, temperature and N/Z asymmetry is of fundamental importance for the understanding of many phenomena involving nuclear systems and astrophysical compact objects. This information can be accessed by mean of heavy ion collision experiments, where transient states of nuclear matter spanning a large variety of regimes can be created. Actually this study allows one to learn about the corresponding behavior of the nuclear effective interaction, which provides the nuclear Equation of State (EOS) in the equilibrium limit. Over the past years, measurements of experimental observables, like isoscalar collective vibrations, collective flows and meson production, have contributed to constrain the EOS of symmetric matter for densities up to five time the saturation value [1]. More recently, the availability of exotic beams has made it possible to explore, in laboratory conditions, new aspects of nuclear structure and dynamics up to extreme ratios of neutron (N) to proton (Z) numbers, also opening the way to the investigation of the EOS of asymmetric matter, which has comparatively few experimental constraints. Indeed, the isovector part of the nuclear effective interaction and the corresponding symmetry energy of the EOS (Asy-EOS) are largely unknown as soon as we move away from normal density, especially in the high density regime.

Nevertheless, this information is essential in the astrophysical context, for the understanding of the properties of compact objects such as neutron stars, whose crust behaves as low-density asymmetric nuclear matter [2] and whose core may touch extreme values of density and asymmetry. Moreover, the low-density behavior of the symmetry energy also affects the

structure of exotic nuclei and the appearance of new features involving the neutron skin, which are currently under intense investigation [3].

Over the past years, several observables which are sensitive to the Asy-EOS and testable experimentally, have been suggested [4, 5, 6, 7]. In this article we will review recent results on dissipative collisions in a wide range of beam energies, from just above the Coulomb barrier up to the AGeV range, on the basis of transport theories of the Stochastic Mean Field (SMF) type. Low energies will bring information on the symmetry term around (below) normal density, while intermediate energies will probe high density regions.

2. Transport theories and symmetry energy

Nuclear reactions are modeled by solving transport equations based on mean field theories, with short range (2p-2h) correlations included via hard nucleon-nucleon elastic collisions and via stochastic forces, selfconsistently evaluated from the mean phase-space trajectory, see [8, 5]. Stochasticity is essential in order to get distributions as well as to allow for the growth of dynamical instabilities.

In the energy range up to a few hundred A MeV, the appropriate tool is the so-called Boltzmann-Langevin (BL) equation [8]:

$$\frac{df}{dt} = \frac{\partial f}{\partial t} + \{f, H\} = I_{coll}[f] + \delta I[f], \tag{1}$$

where $f(\mathbf{r}, \mathbf{p}, t)$ is the one-body distribution function, the semi-classical analog of the Wigner transform of the one-body density matrix, $H(\mathbf{r}, \mathbf{p}, t)$ the mean field Hamiltonian, I_{coll} the two-body collision term incorporating the Fermi statistics of the particles, and $\delta I[f]$ its fluctuating part. Here we follow the approximate treatment of the BLE introduced in Ref. [9], the Stochastic Mean Field (SMF) model. The numerical procedure to integrate the transport equations is based on the test-particle method.

Effective interactions (associated with a given EOS) can be considered as an input of the transport code and from the comparison with experimental data one can finally get some hints on the properties of the nuclear interaction.

We recall that the symmetry energy E_{sym} appears in the energy density functional $\epsilon(\rho, \rho_i) \equiv \epsilon(\rho) + \rho\frac{E_{sym}}{A}(\rho_i/\rho)^2 + O(\rho_i/\rho)^4 + ..$, expressed in terms of total ($\rho = \rho_p + \rho_n$) and isospin ($\rho_i = \rho_p - \rho_n$) densities. E_{sym} gets a kinetic contribution directly from basic Pauli correlations and a potential part, $C(\rho)$, from the highly controversial isospin dependence of the effective interactions:

$$\frac{E_{sym}}{A} = \frac{E_{sym}}{A}(kin) + \frac{E_{sym}}{A}(pot) \equiv \frac{\epsilon_F}{3} + \frac{C(\rho)}{2\rho_0}\rho \tag{2}$$

(ρ_0 denotes the saturation density). The nuclear mean-field, consistently derived from the energy functional, can be written as:

$$U_q = A\frac{\rho}{\rho_0} + B(\frac{\rho}{\rho_0})^{\alpha+1} + C(\rho)\frac{\rho_n - \rho_p}{\rho_0}\tau_q + \frac{1}{2}\frac{\partial C}{\partial \rho}\frac{(\rho_n - \rho_p)^2}{\rho_0}, \tag{3}$$

where $\tau_q = +1(-1)$ for $q = n(p)$. The isoscalar section is fixed requiring that the saturation properties of symmetric nuclear matter, with a compressibility modulus around $K = 200$ MeV [1], are reproduced (which corresponds to the Skyrme SKM* effective interaction). The corresponding values of the coefficients are $A = -356.8$ MeV, $B = 303.9$ MeV, $\alpha = 1/6$.

The sensitivity of the simulation results is tested against different choices of the density dependence of the isovector part of the effective interaction. We employ three different parameterizations of $C(\rho)$: the asysoft, the asystiff and asysuperstiff respectively, see [5] for a detailed description. The value of the symmetry energy, E_{sym}/A, at saturation, as well as the

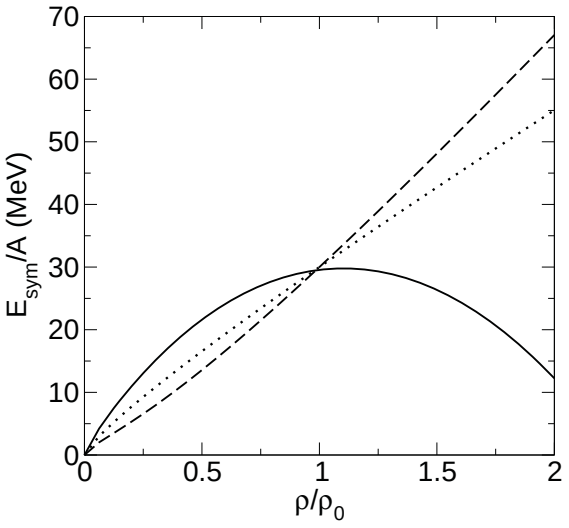

Figure 1. Three effective parameterizations of the symmetry energy : asystiff (dotted line), asysoft (full line) and asysuperstiff (dashed line).

slope parameter, $L = 3\rho_0 \frac{dE_{sym}/A}{d\rho}|_{\rho=\rho_0}$, are reported in table 1 (first two columns) for each of these Asy-EOS. Just below the saturation density the asysoft mean field has a weak variation with density while the asysuperstiff shows a rapid decrease, see figure 1.

For protons, the Coulomb interaction is also included in the simulations.

Surface terms are not explicitly included in the mean-field potential, however surface effects are accounted for by considering finite width wave packets for the test particles employed in the numerical resolution of equation (1). The width is tuned to reproduce the surface energy of nuclei in the ground state [10]. This method also induces the presence of a surface term in the symmetry energy. We have checked that properties connected to surface effects, such as the neutron skin of neutron-rich nuclei, are in reasonable agreement with calculations of other models employing similar interactions [11, 12].

Momentum-dependent effective interactions may also be implemented into equation (1) and will be considered in the following for the study of observables which are particularly sensitive to this ingredient. In particular, we will discuss results related to the momentum dependence of the isovector channel of the interaction, leading to the splitting of neutron and proton effective masses (see section 4).

3. Collective excitations in neutron-rich systems

One of the important tasks in many-body physics is to understand the emergence of collective features as well as their structure in terms of the individual motion of the constituents. The experimental characterization and theoretical description of collective excitations appearing in charge asymmetric and exotic systems is a challenge for modern nuclear physics.

3.1. New exotic collective excitations

Recent experiments of Coulomb dissociation have provided several evidences about the existence of new collective excitations in neutron-rich systems, but the available information is still incomplete and their nature is a matter of debate. In particular, many efforts have been devoted to the study of the Pygmy Dipole Resonance (PDR), identified as an unusually large concentration of the isovector dipole response at energies below the values corresponding to the Giant Dipole Resonance (GDR). The latter is one of the most prominent and robust collective motions, present in all nuclei, whose centroid position varies, for medium-heavy nuclei, as $80A^{-1/3}$ MeV. From a comparison of the available data for stable and unstable Sn isotopes

Table 1. The symmetry energy at saturation (in MeV), the slope parameters, neutron rms radius, protons rms radius, neutron skin thickness of ^{132}Sn for the three Asy-EOS.

asy-EoS	E_{sym}/A	L(MeV)	R_n(fm)	R_p(fm)	ΔR_{np}(fm)
asysoft	29.9	14.4	4.90	4.65	0.25
asystiff	28.3	72.6	4.95	4.65	0.30
asysupstiff	28.3	96.6	4.96	4.65	0.31

a correlation between the fraction of pygmy strength and isospin asymmetry was noted [13]. In general the exhausted sum-rule increases with the proton-to-neutron asymmetry. This behavior was related to the symmetry energy properties below saturation and therefore connected to the size of the neutron skin [14, 3].

In spite of the theoretical progress in the interpretation of this mode and new experimental information [15, 16, 17, 18], a number of critical questions concerning the nature of the PDR still remains. Here we want to address the important issue related to the collective nature of the PDR in connection with the role of the symmetry energy.

A microscopic, self-consistent study of the collective features and of the role of the nuclear effective interaction upon the PDR can be performed within the Landau theory of Fermi liquids. This is based on two coupled Vlasov kinetic equations (see equation (1), neglecting two-body correlations) for neutron and proton one-body distribution functions $f_q(\mathbf{r}, \mathbf{p}, t)$ with $q = n, p$, and was applied quite successfully in describing various features of the GDR, including pre-equilibrium dipole excitation in fusion reactions [19]. However, it should be noticed that within such a semi-classical description shell effects are absent, certainly important in shaping the fine structure of the dipole response [20]. By solving numerically the Vlasov equation, in the absence of Coulomb interaction, Urban [21] evidenced from the study of the total dipole moment D a collective response around 8.6 MeV which was identified as a pygmy mode. Here, considering in the transport simulations also the Coulomb interaction, we explore the isoscalar character of the mode by a comparative analysis, employing the three different density parametrizations of the symmetry energy introduced above (see figure 1).

One of the most important goals is to address the connection between the development of the neutron skin and the emergence of a low-energy E1 response, a subject under intense debate during the last years. Since, as in the case of the GDR, the evolution with mass of the low-energy E1 response provides an additional insight into the nature of the mode, we shall consider the systems ^{48}Ca, ^{68}Ni, ^{86}Kr and ^{208}Pb, as well as a chain of Sn isotopes, $^{108,116,124,132,140}Sn$.

From the one-body distribution functions one obtains the local densities in the ground state: $\rho_q(\vec{r}, t) = \int \frac{2d\mathbf{p}}{(2\pi\hbar)^3} f_q(\mathbf{r}, \mathbf{p}, t)$ as well as the quadratic radii $\langle r_q^2 \rangle = \frac{1}{N_q} \int d\mathbf{r}\ r^2 \rho_q(\mathbf{r}, t)$ and the width of the neutrons skin $\Delta R_{np} = \sqrt{\langle r_n^2 \rangle} - \sqrt{\langle r_p^2 \rangle} = R_n - R_p$.

The integration of the transport equations is based on the test-particle (t.p.) method, with a number of 1300 t.p. per nucleon, ensuring in this way a good spanning of the phase-space.

An efficient method to extract the values of R_n and R_p is by observing their time evolution after a gentle perturbation. Both quantities perform small oscillations around equilibrium values and we remark that the numerical simulations keep a very good stability of the dynamics for at least 2000 fm/c. Using this procedure we obtain for the charge mean square radius of ^{208}Pb a value around $R_p = 5.45$ fm, to be compared with the experimental value $R_{p,exp} = 5.50$ fm. For Sn isotopes we display the mass dependence of R_n, R_p in figure 2 (a) and of ΔR_{np} respectively in figure 2 (b). Values for ^{132}Sn are also reported in table 1. For the charge radii the predictions from the three Asy-EOS virtually coincide and we notice a good agreement with the experimental

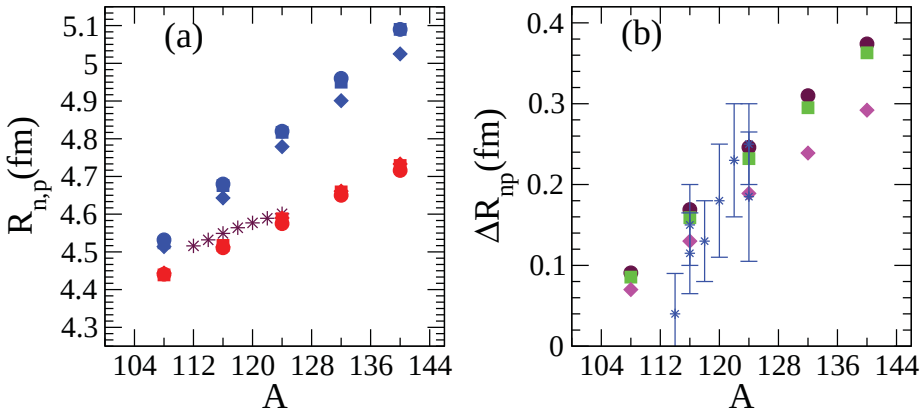

Figure 2. (Color online) (a) The neutron (blue) and proton (red) mean-square radius for Sn isotopes: asysoft (diamonds), asystiff (squares) and asysuperstiff (circles) EOS. The stars are experimental data from Refs. [22]. (b) The neutron skin size as a function of mass for Sn isotopes: asysoft (magenta diamonds), asystiff (green squares), asysuperstiff (maroon circles). The stars and the error bars (blue) are experimental data from Ref. [23].

data reported in [22]. For all adopted parametrizations the predicted values of the neutron skin thickness are within the experimental errors bars, see the data presented in [23] for the stable Sn nuclei. In the case of ^{208}Pb we find $\Delta R_{np} = 0.19$ fm for asysoft, $\Delta R_{np} = 0.25$ fm for asystiff and $\Delta R_{np} = 0.27$ fm for asysuperstiff, whereas for ^{68}Ni the corresponding values are $\Delta R_{np} = 0.17, 0.19, 0.20$ fm. We see that the neutron skin thickness increases with the slope parameter L, an effect related to the tendency of the system to stay more isospin symmetric even at lower densities when the symmetry energy changes slowly below saturation, as in the case of the asysoft EOS.

3.2. Results of transport approaches

We study the E1 response considering a GDR-like initial condition [24], determined by the instantaneous excitation $V_{ext} = \eta\delta(t-t_0)\hat{D}$ at $t = t_0$ [25]. This situation corresponds to a boost of all neutrons against all protons while keeping the Center of Mass (CM) at rest. Here $\hat{D}$ is the dipole operator. If $|\Phi_0\rangle$ is the state before perturbation then the excited state becomes $|\Phi(t_0)\rangle = e^{i\eta\hat{D}}|\Phi_0\rangle$ and the value of η can be related to the initial expectation value of the collective dipole momentum $\hat{\Pi}$, $\langle\Phi(t_0)|\hat{\Pi}|\Phi(t_0)\rangle = \hbar\eta\frac{NZ}{A}$. Here $\hat{\Pi}$ is canonically conjugated to the collective coordinate $\hat{X}$ which defines the distance between the CM of protons and neutrons, i.e. $[\hat{X}, \hat{\Pi}] = i\hbar$ [26]. Then the strength function $S(E) = \sum_{n>0}|\langle n|\hat{D}|0\rangle|^2\delta(E_n - E_0)$, directly related to the excitation probability in unit time (where E_n are the excitation energies of the states $|n\rangle$ and E_0 is the energy of the ground state $|0\rangle = |\Phi_0\rangle$), is obtained from the imaginary part of the Fourier transform of the time-dependent expectation value of the dipole momentum $D(t) = \frac{NZ}{A}X(t) = \langle\Phi(t)|\hat{D}|\Phi(t)\rangle$, as $S(E) = \frac{Im(D(\omega))}{\pi\eta\hbar}$. We consider the initial perturbation along the z-axis and follow the dynamics of the system until $t_{max} = 1830$ fm/c in each case. At $t = t_0 = 30$ fm/c we extract the collective momentum and determine η. For the three Asy-EOS the E1 strength functions of ^{208}Pb and ^{140}Sn are represented in figure 3. As a test of the quality of our method we compared the numerically estimated value of the first moment $m_1 = \int_0^\infty ES(E)dE$ with the value predicted by the Thomas-Runke-Kuhn (TRK) sum rule

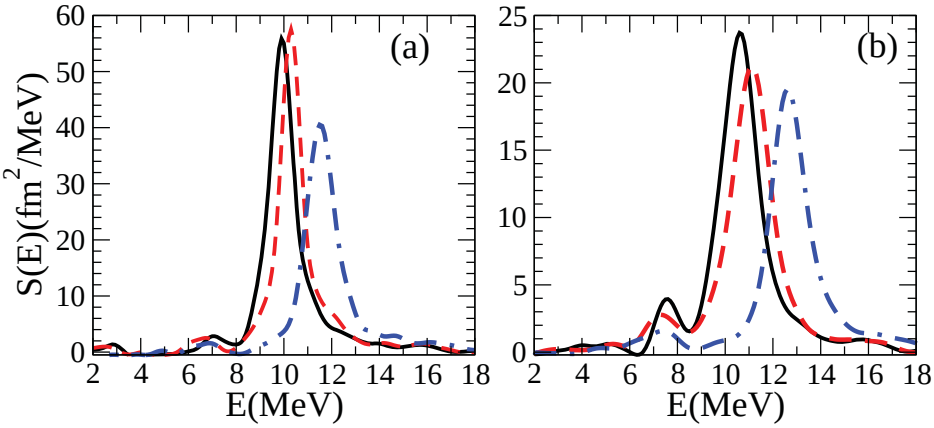

Figure 3. (Color online) The strength function for ^{208}Pb (a) and ^{140}Sn (b) for asysoft (blue, dot-dashed line), aystiff (red, dashed line) and asysuperstiff (black, solid line) EOS.

$m_1 = \frac{\hbar^2}{2m}\frac{NZ}{A}$. In all cases the difference was of only few percentages. The energy peak of the PDR for ^{208}Pb, see figure 3(a), is located around $7 - 7.5$ MeV in good agreement with recent experimental data which indicate $E_{PDR,Pb} = 7.36$ MeV [27]. For ^{68}Ni we obtain 9.8 MeV, quite close to the recent reported data $E_{PDR,Ni} = 9.9$ MeV [28]. We observe that the GDR energy centroid is underestimated in comparison with experimental data, a fact probably related to the choice of the interaction which has not an effective mass [29]. In any case, a clear dependence with the slope parameter L manifests as a consequence of the isovector nature of the mode. This feature shows that the symmetry energy behavior below saturation is also affecting the dipole oscillations of finite systems. Figure 4 displays the position of the PDR energy centroid, which is independent of the Asy-EOS, as a function of mass for all studied systems (blue circles). In addition, we represent the position of the PDR energy peak as it results from the power spectrum analysis of the pygmy dipole $D_y(t)$ after a pygmy-like initial condition, see [24] (red diamonds), and the available experimental data (maroon square) [30]. The differences between the two methods are within a half of MeV. An appropriate parametrization, obtained from the fit of the numerical results is $E_{PDR} = 41A^{-1/3}$, quite close to what is expected in the harmonic oscillator shell model (HOSM) approach [26] and in agreement with some recent experimental data. Whereas the isovector residual interaction pushes up the value of the GDR energy it seems that the PDR energy centroid is not much affected by this part of the interaction, indicating the isoscalar-like nature of this mode. This feature may explain the better agreement with experimental observations in comparison with the GDR case. Let us mention that for Ni, Sn and Pb isotopic chains, the isotopic dependence of the PDR energy was also investigated by Paar *et al.* [38], within a HFB and RQRPA treatment. The presence of a collective mode with energy centroid around 10 MeV for ^{68}Ni, 8 MeV for ^{132}Sn and 7.5 MeV for ^{208}Pb was predicted. A comparison with our results shows a good agreement between the two theoretical approaches.

We can now determine the Energy Weighted Sum Rule (EWSR) exhausted by the PDR by integrating over the low-energy resonance region:

$$m_{1,y} = \int_{PDR} ES(E)dE \tag{4}$$

The dependence of the moment $m_{1,y}$ on the neutron skin thickness is shown in figure 5, where the information concerning all mentioned systems for the three Asy-EOS is included. While below 0.15 fm the EWSR acquired by the PDR manifests a saturation tendency, above this value a

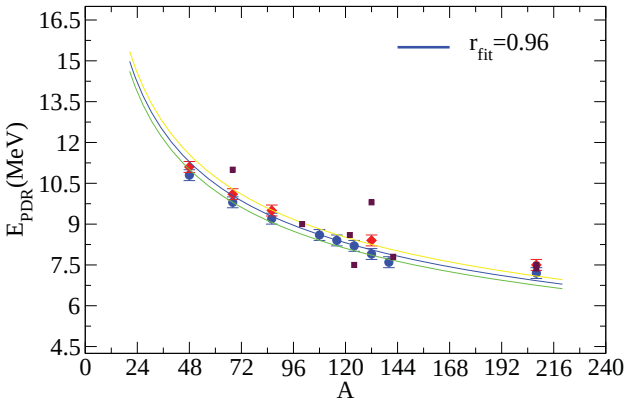

Figure 4. (Color online) The energy centroid of PDR as a function of mass (blue circles and red diamonds). The solid lines correspond to parametrizations $40A^{-1/3}$ (green), $41A^{-1/3}$ (blue) and $42A^{-1/3}$ (yellow). The maroon squares are experimental data from Ref. [30]. r_{fit} refers to the correlation coefficient.

linear correlation clearly manifests. For the same system, when we pass from asysuperstiff to asysoft parametrisation, the neutron-skin shrinks and correspondingly the value of $m_{1,y}$ decreases. This behavior is in agreement with the results reported in [39] with a self-consistent RPA approximation based on relativistic energy density functionals. Moreover we notice that the variation rate appears to be system independent, obtaining an increase of 15 MeV fm^2 of the exhausted EWSR to a change of 0.1 fm of the neutron skin width. Such features suggest that the acquired EWSR should not differ too much even for different nuclei if they have close values of the neutrons skin thickness. We would like to mention that these findings look qualitatively in agreement with those of Inakura [40], based on systematic RPA calculations.

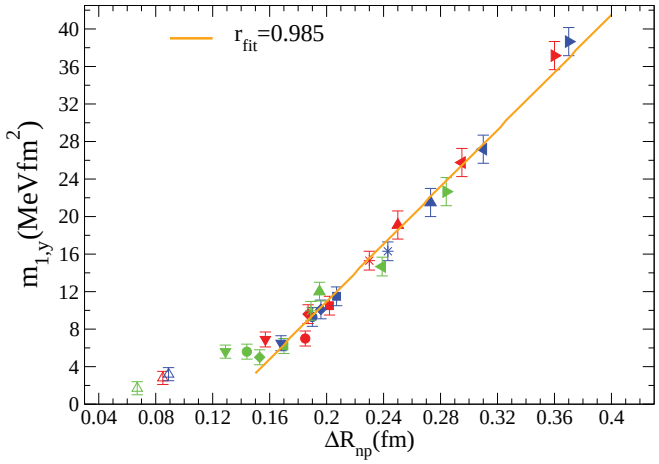

Figure 5. (Color online) The EWSR exhausted by PDR as a function of neutron skin in ^{108}Sn (empty triangles up), ^{116}Sn (triangles down), ^{124}Sn (stars), ^{132}Sn (triangles left), ^{140}Sn (triangles right), ^{48}Ca (circles), ^{68}Ni (squares), ^{86}Kr (diamonds), ^{208}Pb (full triangles up), for asysoft (green), asystiff (red) and asysuperstiff (blue) EOS. r_{fit} refers to the correlation coefficient. The error bars are related to the uncertainties in defining the integration domain for the PDR response.

To conclude this section, we have discussed recent open questions [41] regarding the nature of the PDR. By performing a systematic analysis which includes several nuclear systems we obtained new results aiming at contributing to a more complete picture of the PDR dynamics. In a microscopic transport approach, a low-energy dipole collective mode is evidenced as an ubiquitous feature of all investigated nuclei. The analysis leads to a dependence of the PRD energy centroid with mass described by $E_{PDR} = 41A^{-1/3}$, in agreement with recent experimental information. This indicates a close connection with the characteristic frequency of the HOSM, $\hbar\omega_0 = 41A^{-1/3}$, and a weak influence of the residual interaction in the isovector sector [42]. Such behavior points out the isoscalar-like nature of this mode. From our calculations a universal, linear correlation of the EWSR exhausted by PDR with the neutron skin thickness occurs [43].

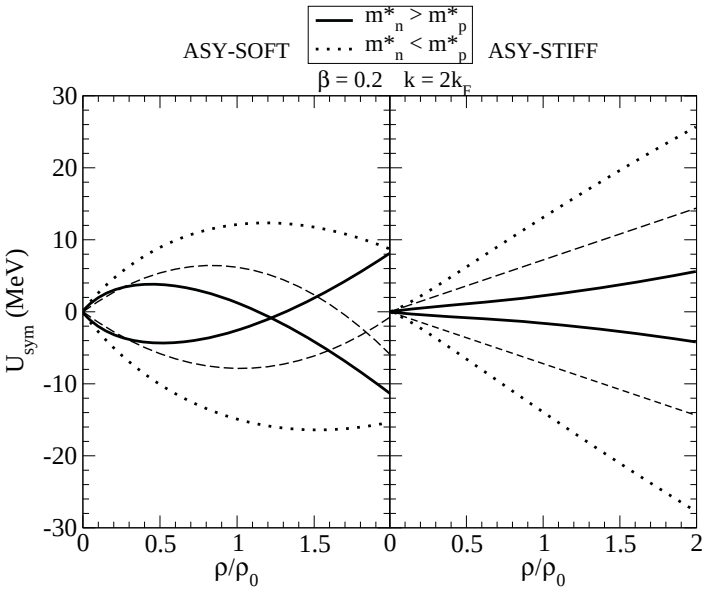

Figure 6. Density dependence of neutron(upper)-proton(lower) potentials for an asymmetry $\beta = (N-Z)/(N+Z) = 0.2$ for the asysoft (left) and asystiff (right) choices. Dashed: No momentum dependence. Momentum dependent potentials at momentum $k = 2k_F$: solid lines for the $m_n^* > m_p^*$ case, dotted lines for the opposite $m_n^* < m_p^*$ choice.

It appears as a very specific signature, showing that the neutrons which belong to the skin play an essential role in shaping the E1 response in the PDR region. We consider that the new findings presented here can be useful for further systematic experiments searching for this quite elusive mode. A precise estimate of the EWSR acquired by the PDR can provide indications about the neutron skin size which in turn will add more constraints on the slope parameter L of the symmetry energy.

4. Asy-EOS at supra-saturation density: collective flows

Reactions with neutron-rich systems at intermediate energies (100-500 AMeV) are of interest in order to have high momentum particles and to test regions of high baryon and isovector density during the reaction dynamics. In such a context, it is important to consider momentum dependent effective interactions, which essentially lead to the concept of effective masses. If also the isovector component of the interaction is momentum dependent, one observes different effective masses (i.e. effective mass splitting) for neutrons and protons. The problem of the precise determination of the Momentum Dependence in the Isovector channel ($Iso-MD$) of the nuclear interaction is still very controversial and it would be extremely important to get more definite experimental information, looking at observables which may also be sensitive to the mass splitting.

Transport codes are usually implemented with different (n,p) momentum dependent interactions, see for instance [44, 45]. This allows one to follow the dynamical effect of opposite n/p effective mass (m^*) splitting while keeping the same density dependence of the symmetry energy [46]. Neutron and proton symmetry potentials, corresponding to different symmetry energy parametrizations and effective mass splitting, are represented as a function of the density in figure 6. One can observe an interesting competition between the two ingredients: above normal density, for instance, the asysoft parametrization, coupled to the $m_n^* < m_p^*$ splitting, leads to similar potentials as obtained in the asystiff case, with $m_p^* < m_n^*$.

Let us consider semicentral ($b/b_{max} = 0.5$) collisions of $^{197}Au + ^{197}Au$ at 400 AMeV [47]. In the interacting zone baryon densities about $1.7-1.8\ \rho_0$ can be reached in a transient time of the order of 15-20 fm/c. The system is quickly expanding and the freeze-out time is around 50 fm/c. A rather abundant particle emission is observed over this time scale. Here it is very interesting to study again the collective response of the system. Collective flows are very good candidates

since they are expected to be rather sensitive to the momentum dependence of the mean field, see [48, 5]. The transverse flow, $V_1(y, p_t) = \langle \frac{p_x}{p_t} \rangle$, where $p_t = \sqrt{p_x^2 + p_y^2}$ is the transverse momentum and y the rapidity along the beam direction, provides information on the anisotropy of nucleon emission on the reaction plane. Very important for the reaction dynamics is also the elliptic flow, $V_2(y, p_t) = \langle \frac{p_x^2 - p_y^2}{p_t^2} \rangle$. The sign of V_2 indicates the azimuthal anisotropy of the emission: on the reaction plane ($V_2 > 0$) or out-of-plane ($squeeze - out,\ V_2 < 0$) [48].

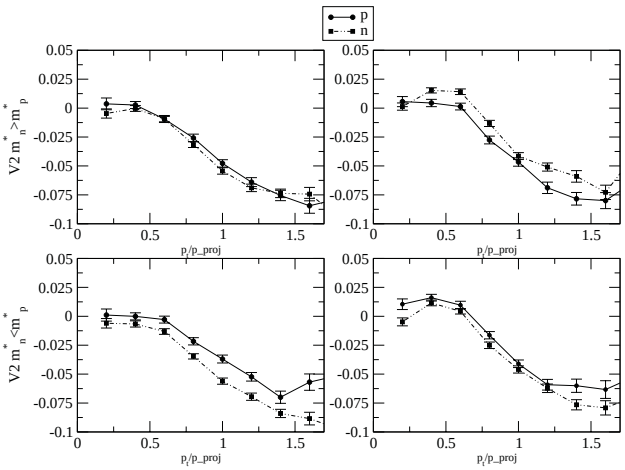

Figure 7. Proton (thick) and neutron (thin) V_2 flows in a semi-central reaction $Au + Au$ at 400 AMeV. Transverse momentum dependence at midrapidity, $\mid y_0 \mid < 0.3$. Upper curves for $m_n^* > m_p^*$, lower curves for the opposite splitting $m_n^* < m_p^*$. Left: asystiff. Right: asysoft.

In figure 7, we plot the elliptic flow of emitted neutrons and protons, for different asy-stiffness and effective mass splitting choices. We are now exploring density regions mainly above normal density, therefore we expect a larger neutron repulsion in the asystiff case, corresponding to the larger symmetry energy value (see figure 1). Indeed in figure 7 we observe a larger (negative) squeeze-out for neutrons in the asystiff case (compare left and right panels). Moreover, the $m_n^* < m_p^*$ case will favor the neutron repulsion, leading to a larger squeeze-out for neutrons, compare top and bottom panels. In particular, in the asysoft case (on the right) we see an inversion of the neutron/proton squeeze-out at mid-rapidity ($|y_0| = |y/y_{beam}| < 0.3$) for the two effective mass-splittings.

Actually, we observe a rather interesting interplay between the effects linked to the symmetry energy and to the mass splitting, connected to the behavior of neutron and proton potentials described above: a larger (smaller) neutron effective mass may compensate the larger (smaller) neutron repulsion corresponding to the asystiff (asysoft) case. Indeed the $m_n^* < m_p^*$ case, with the soft Asy-EOS, yields very similar results of the $m_p^* < m_n^*$ case with the stiff Asy-EOS.

It seems to be difficult to conclude on the properties of the effective interaction (asystiffness and MD) just from the analysis of one single observable. However, coupling the flow information to the study of other observables, it would be possible to reach more definitive constraints of the effective interaction. For instance, in the considered beam energy range, the N/Z content of the particle emission looks particularly sensitive just to the sign of mass splitting, rather than to the asy-stiffness [47]. Indeed pre-equilibrium particles emerge from different density regimes and the effect of the density dependence of the isovector interaction is averaged out. This is illustrated in figures 8-9, where we plot the ratio of neutrons and protons emitted at mid-rapidity, as a function of transverse momentum or energy.

Hence it would be very interesting the combine the information coming from particle flows and yields. Recent experimental analyses look very promising in this direction [49, 50]. Due to the difficulties in measuring neutrons, one could also investigate the difference between light isobar (like ^{3}H vs. ^{3}He) flows and yields, also shown in figures 8-9. We still expect to see effective

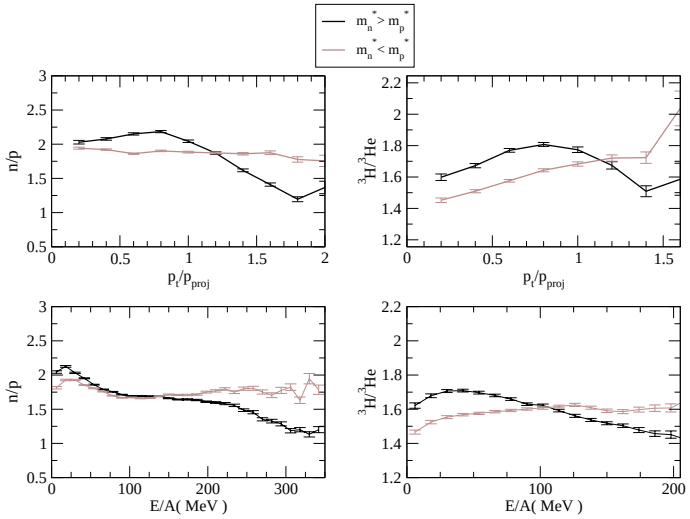

Figure 8. $^{197}Au + ^{197}Au$ at 400 AMeV, central collisions. Isospin content of nucleon (left) and light ion (right) emissions vs. p_t at midrapidity, $\mid y_0 \mid < 0.3$, (upper) and kinetic energy (lower), for all rapidities, for the two nucleon mass splitting choices. Asysoft interaction.

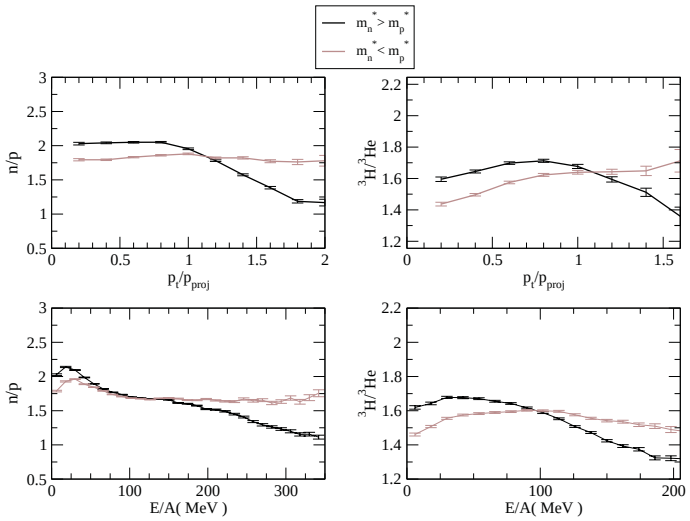

Figure 9. Same as in figure 8, but for the asystiff interaction.

mass splitting effects [47].

5. Conclusions

Heavy ion reactions, from low up to intermediate energies, allow one to explore several regimes of nuclear matter, opening the possibility to constrain the nuclear EOS and, in particular, the largely debated density behavior of the symmetry energy.

Information on the low density region can be accessed in reactions from low to Fermi energies, where collective excitations and fragmentation mechanisms are dominant. Results on isospin sensitive observables have been presented. In particular, we have concentrated our analysis on the features of collective dipole oscillations in exotic systems, showing an interesting correlation between the strength exhausted by the "pygmy" dipole resonance and the extension of the neutron skin, which in turn reflects the behavior of the symmetry energy below normal density. The conclusions drawn from this analysis seem to be compatible with the information extracted

from fragmentation reactions and related observables, for which new experimental evidences have recently appeared, pointing towards a stiff behavior of the symmetry energy around normal density [51, 52].

The greatest theoretical uncertainties concerns the high density domain, that has the largest impact on the understanding of the properties of neutron stars. This regime can be explored in terrestrial laboratories by using intermediate energy and relativistic heavy ion collisions of charge asymmetric nuclei. Collective flows, light particle and meson production are promising observables.

More global analyses, also based on new sensitive observables, together with the comparison and the improvement of the available theoretical models, are expected to improve our present knowledge, providing further stringent constraints.

Acknowledgements
This work for Baran V was supported by a grant of the Romanian National Authority for Scientific Research, CNCS - UEFISCDI, project number PN-II-ID-PCE-2011-3-0972.

References

[1] Danielewicz P, Lacey R, and Lynch W G 2002 *Science* **298** 1592
[2] Lattimer J M and Prakash M 2007 *Phys. Rep.* **442** 109
[3] Piekarewicz J 2006 *Phys. Rev. C* **73** 044325
[4] *Isospin Physics in Heavy-ion Collisions at Intermediate Energies*, Eds. Li B A and Schröder W U, Nova Science Publishers (2001, New York)
[5] Baran V, Colonna M, Greco V, and Di Toro M 2005 *Phys. Rep.* **410** 335
[6] Colonna M and Tsang M B 2006 *Eur. Phys. J. A* **30** 165, and references therein
[7] Li B A, Chen L W, and Ko C M 2008 *Phys. Rep.* **465** 113
[8] Chomaz P, Colonna M, and Randrup J 2004 *Phys. Rep.* **389** 263
[9] Colonna M *et al.* 1998 *Nucl. Phys. A* **642** 449
[10] Guarnera A, Colonna M, and Chomaz Ph 1996 *Phys. Lett. B* **373** 267
[11] Baran V, Frecus B, Colonna M, and Di Toro M 2012 *Phys. Rev. C* **85** 051601(R)
[12] Paar N, Nicsik T, Vretenar D, and Ring P 2005 *Phys. Lett. B* **606** 288
[13] Klimkiewicz A *et al.* 2007 *Phys. Rev. C* **76** 051603(R)
[14] Yoshida S and Sagawa H 2004 *Phys. Rev. C* **69** 024318; 2006 *Phys. Rev. C* **73** 044320
[15] Savran D *et al.* 2008 *Phys. Rev. Lett.* **100** 232501
[16] Wieland O *et al.* 2010 *Phys. Rev. Lett.* **102** 092502; Wieland O and Bracco A 2011 *Prog. Part. Nucl. Phys.* **66** 304; Toft H K *et al.* 2010 *Phys. Rev. C* **81** 064311
[17] Tonchev A P *et al.* 2010 *Phys. Rev. Lett.* **104** 072501
[18] Makinaga A *et al.* 2010 *Phys. Rev. C* **82** 024314
[19] Baran V, Rizzo C, Colonna M, Di Toro M, and Pierroutsakou D 2009 *Phys. Rev. C* **79** 021603(R)
[20] Roca-Maza X, Pozzi G, Brenna M, Mizuyama K, and Colò G 2012 *Phys. Rev. C* **85** 024601
[21] Urban M 2012 *Phys. Rev. C* **85** 034322
[22] De Jager C W *et al.* 1987 *At. Data Nucl. Data Table* **36** 495; Audi G and Wapstra A H 1995 *Nucl. Phys. A* **595** 409
[23] Krasznahorkay A *et al.* 1999 *Phys. Rev. Lett.* **82** 3216
[24] Baran V, Frecus B, Colonna M, and Di Toro M 2012 *Phys. Rev. C* **85** 051601
[25] Calvayrac F, Reinhard P G, and Suraud E 1997 *Ann. Phys.* **225** 125
[26] Abrosimov V I and Davydovs'ka O I 2009 *Ukr. J. Phys.* **54** 1068; Baran V *et al.* 2012 *Rom. J. Phys.* **57** 36
[27] Tamii A *et al.* 2011 *Phys. Rev. Lett.* **107** 062502
[28] Rossi D 2014 *INPC2013 Proceedings* and private communication
[29] Suraud E, Pi M, and Schuck P 1988 *Nucl. Phys. A* **482** 187c
[30] For ^{68}Ni from [31]; for ^{100}Mo from [32]; for ^{122}Sn from [33]; for ^{124}Sn from [34]; for ^{132}Sn from [35]; for ^{142}Nd from [36]; for ^{208}Pb from [27, 37]
[31] Wieland O *et al.* 2009 *Phys. Rev. Lett.* **102** 092502
[32] Rusev G *et al.* 2006 *Eur. Phys. J. A* **27** 171

[33] Toft H K *et al.* 2011 *Phys. Rev. C* **83** 044320
[34] Endres J *et al.* 2010 *Phys. Rev. Lett.* **105** 212503
[35] Adrich P *et al.* 2005 *Phys. Rev. Lett.* **95** 132501
[36] Angell C T *et al.* 2012 *Phys. Rev. C* **86** 051302(R)
[37] Kondo T *et al.* 2012 *Phys. Rev. C* **86** 014316
[38] Paar N *et al.* 2005 *Phys. Lett. B* **606** 288
[39] Vretenar D *et al.* 2012 *Phys. Rev. C* **85** 044317
[40] Inakura T *et al.* 2011 *Phys. Rev. C* **84** 021302(R)
[41] Savran D, Aumann T, and Zilges A 2013 *Prog. Part. Nucl. Phys.* **70** 210
[42] Lanza E *et al.* 2011 *Phys. Rev. C* **84** 064602
[43] Baran V *et al.* 2013 *Phys. Rev. C* **88** 044610
[44] Li B A, Das Champak B, Das Gupta S, and Gale C 2004 *Nucl. Phys. A* **735** 563
[45] Rizzo J, Colonna M, and Di Toro M 2005 *Phys. Rev. C* **72** 064609
[46] Rizzo J *et al.* 2008 *Nucl. Phys. A* **806** 79
[47] Giordano V *et al.* 2010 *Phys. Rev. C* **81** 044611
[48] Danielewicz P 2000 *Nucl. Phys. A* **673** 375
[49] Russotto P *et al.* 2011 *Phys. Lett. B* **697** 471
[50] Cozma M D 2011 *Phys. Lett. B* **700** 139
[51] De Filippo E *et al.* (Chimera Collaboration) 2012 *Phys. Rev. C* **86** 014610
[52] Tsang M B *et al.* 2012 *Phys. Rev. C* **86** 015803